

Unveiling the Multifaceted Nature of 4-(4-Methylphenyl Thio)benzophenone: A Combined DFT, NBO, and Spectroscopic Investigation of its Electronic Structure and Excited States

Manjeet Bhatia*

*QuantumSIMM, Kangra, Himachal Pradesh, 177105, India

www.quantumsimm.com

Email: manjeetbhatia83@gmail.com

Abstract

Benzophenone and its derivatives play a crucial role as UV (ultra-violet) filters and UV-ink photoinitiators. The photoinitiating properties of benzophenones are primarily linked to the degree of π -conjugation and the extent of delocalization within the molecule. Understanding the intricate interplay of conjugation, delocalization, and substituent effects allows for the precise customization of benzophenone derivatives to meet specific application requirements. Quantum mechanical calculations, employing the B₃LYP/6-311++G(d, p) density functional theory (DFT), are utilized to compute chemical reactivity, stability, and photoinitiating properties for 4-(4-methylphenylthio) benzophenone. Various parameters such as proton affinity, ionization energy, electron affinity, reactivity, and spectroscopic properties are determined. The DFT-computed infrared spectra align well with available experimental results. The UV/Visible spectra obtained using TD-DFT reveal absorption toward higher wavelengths, attributed to the extended delocalization of π -electrons. In an aqueous medium, the absorption spectra of 4-(4-methylphenylthio) benzophenone exhibit a high-intensity peak with a longer wavelength shift in the visible region compared to gas-phase spectra. This knowledge provides the foundation for designing novel initiators with tailored light absorption, excited state lifetimes, and reaction selectivities. Consequently, these advancements open doors to benefits in UV-curing, photopolymerization, and other light-driven processes.

Keywords: Benzophenones, photoinitiators, UV/Vis spectra, photopolymerization, DFT, chemical reactivity

1. Introduction

The world of materials dances to the silent symphony of light. Within this mesmerizing choreography, benzophenone-based photoinitiators play a starring role, orchestrating the intricate union of molecules under the spotlight of UV (ultra violet) or visible radiation [1, 2]. These remarkable tools, often referred to as the workhorses of photopolymerization, have ignited the

creation of countless materials that enrich our lives, from gleaming coatings and sturdy adhesives to delicate microfluidic devices and intricate 3D printed structures. Benzophenone based derivatives, with its simple yet elegant structure, boasts an almost magical ability to absorb light and undergo a transformation [3]. This excited state fuels a cascade of reactions, triggering the linking of monomers into intricate polymer chains. This remarkable capacity has propelled benzophenone and its derivatives to the forefront of photopolymerization technology, making them the most widely used class of photoinitiators [4]. Benzophenone initiates the curing of various resins and coatings (e.g., inks, adhesives, dental materials) upon exposure to UV light [5, 6, 7]. Benzophenone-based initiators can be incorporated into polymers to trigger their controlled degradation under specific light conditions. Benzophenone derivatives are being explored for photo-regulated drug delivery systems and photodynamic therapy due to their light-activated properties [8, 9].

The quest is on to tailor photoinitiators light absorption, enhance their efficiency, and restrain their unwanted wanderings within materials [10, 11]. Conjugation and delocalization play a significant role in the photoinitiating properties of molecules by influencing their absorption of light, excited state stability, and reactivity. Conjugated molecules with alternating single and double bonds possess extended π -orbital systems. These delocalized π -electrons can efficiently interact with light of specific wavelengths, leading to stronger absorption in the UV or visible region. This increased light absorption is crucial for initiating photochemical reactions, as it triggers the initial excitation of electrons in the molecule. Delocalization of electrons across the conjugated system distributes the excitation energy over a larger area, stabilizing the excited state. This reduces the energy difference between the ground state and the excited state, making the molecule less prone to deactivation through non-productive pathways like fluorescence or internal conversion. Consequently, the excited state lives longer, increasing the probability of it participating in a desired photochemical reaction. Benzophenone and its derivatives remain the most widely used class of photoinitiators due to their effectiveness, broad absorption range, and relative affordability [12, 13, 14]. 4-(4-methylphenylthio)benzophenone (4-4-MPTB) [15, 3, 13], a classic photoinitiator whose conjugated π -system efficiently absorbs light and undergoes excitation, making it widely used in free radical polymerization reactions. Further, electron-donating or withdrawing groups attached to the conjugated system can further influence the light absorption and reactivity of the molecule. Modifying the benzophenone core with electron-donating or withdrawing groups to tune its excited state properties and reactivity. Identifying potential electrophilic, and nucleophilic sites, and π -electron delocalization are crucial for elucidating light absorption and reactivity of the molecule.

Furthermore, solvent effects on UV-Vis spectrometry can be observed through solvatochromic shift in the excited state electronic absorption spectra. This translates to stronger solvent-solute interactions, influencing shifts and intensity. These shifts and intensity changes arise from interactions between the solvent molecules and the solute's electron cloud. Solvents can stabilize or destabilize different excited states, altering their energy levels and consequently, the observed absorption spectrum [16, 17]. Molecular properties along with global reactivity of 4-4-MPTB are computed using DFT and conceptual DFT based on the response functions to the perturbation. These global reactivity descriptors are essential tools in theoretical chemistry, providing valuable information about a molecule's reactivity, stability, and electronic properties [18, 19, 20].

The structure of the article is organized as follows: Section 2 details the computational method used to obtain optimized molecular geometry and other chemical properties. In section 3, the results obtained through density functional theory (DFT) are thoroughly discussed. Finally, conclusions are presented in section 4.

2. Computational Method

The utilized hybrid DFT functional [21], blends exchange contributions from Hartree-Fock theory with correlation contributions from DFT, achieving a commendable equilibrium between accuracy and computational efficiency across a diverse array of properties. These properties encompass geometries, vibrational frequencies, thermochemical characteristics, and electronic structure, including the determination of highest occupied and lowest unoccupied (HOMO/LUMO) orbital energies. The B₃LYP/6-311++G(d, p) method, employed through the Gaussian 16 DFT code [22], serves as the computational framework for assessing the aforementioned molecular properties. This method employs a triple-zeta basis set with polarization functions applied to both heavy atoms (d) and hydrogen atoms (p). Striking a balance between accuracy and computational cost, It delivers reliable results for numerous properties without excessive computational demands. The inclusion of "++" signifies the incorporation of diffuse functions, crucial for describing anions, long-range interactions, and excited states. To ensure the reliability of the results, the molecular structure undergoes geometric relaxation, and vibrational frequency calculations are conducted to confirm the identification of a stationary point, ruling out the presence of imaginary frequencies. The B₃LYP/6-311++G(d, p) combination is known for its consistent and trustworthy performance across various molecular properties [23, 24]. Its relative efficiency, especially when compared to more advanced functionals and basis sets, makes it applicable to a broad spectrum of molecular systems and chemical phenomena.

3. Results and Discussion

Electronic Structure

Employing quantum mechanical calculations, the B₃LYP/6-311++G(d, p) DFT method is applied using Gaussian 16 code to derive the optimized molecular geometry of 4-4-MPTB. Subsequent calculations, including frequency, NBO, HOMO-LUMO, and spectroscopy, are then carried out based on the optimized geometry. Figure 1 illustrates the optimized structure of 4-4-MPTB, while Table 1 provides the corresponding structural parameters.

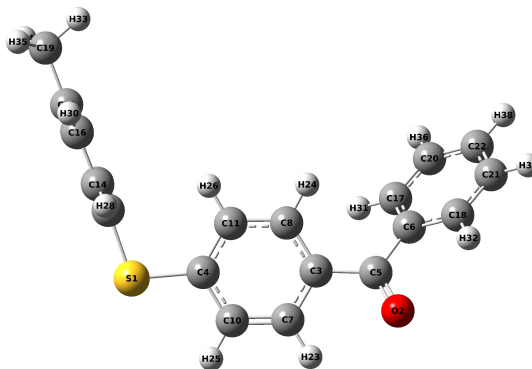


Figure 1. Fully optimized structure of 4-4-MPTB molecule from B₃LYP/6-311++G(d, p) method.

Table 2 presents the DFT-computed molecular properties, encompassing dipole moment, polarizability, proton affinity, ionization energy, electron affinity, and global reactivity parameters. The obtained results indicate a notable dipole moment (5.58 Debye) and substantial polarizability (40.24 Å³), highlighting their significance in elucidating intermolecular interactions and bonding characteristics within the molecule. In mass spectrometry drift tubes, the proton affinity and ionization energy play crucial roles in determining the nature and type of reactions [25]. Global reactivity parameters, including HOMO-LUMO energy, chemical potential (μ), chemical hardness (η), softness (σ), electrophilic index (ω), and electronegativity (χ) are computed as per Koopmans approximation [26]. Koopmans theorem assumes that if adding or removing an electron from a molecule preserves its electronic structure, then the ionization energy and electron affinity can be expressed as $-\epsilon_{\text{HOMO}}$ and $-\epsilon_{\text{LUMO}}$, respectively. Koopmans approximation treats each electron as an independent particle, neglecting electron-electron correlations. Consequently, chemical reactivity parameters are derived from response functions based on orbital energies as outlined in previous studies [27, 28, 29].

$$\mu = -\frac{1}{2}(\text{IP} + \text{EA}) = \frac{1}{2}(\epsilon_{\text{LUMO}} + \epsilon_{\text{HOMO}}) \quad (1)$$

$$\eta = \frac{1}{2}(\text{IP} - \text{EA}) = \frac{1}{2}(\epsilon_{\text{LUMO}} - \epsilon_{\text{HOMO}}) \quad (2)$$

$$\sigma = \frac{1}{2\eta} \quad (3)$$

$$\omega = \mu^2 \sigma \quad (4)$$

Global reactivity descriptors offers provide a condensed overview of molecule's overall reactivity, bypassing the intricacies of specific reaction mechanisms. These descriptors prove invaluable to chemists, providing a swift and convenient means of comparing and contrasting the reactivity of different molecules. They enable the prediction of reaction likelihood and serve as a guide for designing new molecules with desired chemical properties [30, 31]. Frontier molecular orbitals, namely the highest occupied molecular orbital (HOMO) and lowest unoccupied molecular orbital (LUMO), play a pivotal role in comprehending molecule's chemical reactivity. A high HOMO-LUMO energy gap indicates reduced electron susceptibility to move from HOMO to LUMO, rendering the molecule less reactive and more stable. Conversely, a smaller gap suggests easier electron, resulting in higher reactivity for bond formation. Reactivity is contingent upon the ease of gaining or losing electrons, and descriptors such as ionization potential and electron affinity quantify the energy required for these processes. Chemical potential (μ) signifies a molecule's inclination to gain or lose electrons to attain a more stable state. Chemical hardness (η) and chemical softness (σ) encapsulate a molecules's resistant to changes in its electron configuration. Electrophilicity index (ω) predicts a molecules's electrophilic strength, indicating its ability to accept electrons. Electronegativity (χ) measures an atom's propensity to attract electrons towards itself, reflecting its electron-attracting nature.

Table 1. Optimized structural parameters of 4-4-MPTB using B₃LYP/6-311++G(d, p) DFT method.

| Bond | Length | Bond. | Length | Bond | Angle | Bond. | Angle |
|-------------|--------|-------------|--------|-------------|-------|-------------|-------|
| S1-C9 | 1.794 | C10-H25 | 1.085 | S1-C4-C10 | 116.3 | C7-C10-H25 | 119.9 |
| S1-C4 | 1.787 | C11-H26 | 1.082 | S1-C4-C11 | 124.4 | C4-C11-C8 | 119.9 |
| O2-C5 | 1.222 | C12-C16 | 1.400 | C10-C4-C11 | 119.3 | C4-C11-H26 | 120.3 |
| C3-C8 | 1.400 | C12-C15 | 1.399 | O2-C5-C3 | 120.3 | C8-C11-H26 | 120.0 |
| C3-C7 | 1.404 | C12-C19 | 1.509 | O2-C5-C6 | 119.6 | C16-C12-C19 | 121.0 |
| C3-C5 | 1.494 | C13-C15 | 1.393 | C3-C5-C6 | 120.2 | C9-C13-C15 | 120.1 |
| C4-C10 | 1.405 | C13-H27 | 1.084 | C5-C6-C17 | 122.6 | C9-C13-H27 | 120.0 |
| C4-C11 | 1.397 | C14-C16 | 1.392 | C5-C6-C18 | 118.1 | C15-C13-H27 | 120.3 |
| C5-C6 | 1.502 | C14-H28 | 1.084 | C17-C6-C18 | 119.1 | C9-C14-C16 | 120.1 |
| C6-C17 | 1.401 | C15-H29 | 1.085 | C3-C7-C10 | 120.9 | C9-C14-H28 | 120.0 |
| C6-C18 | 1.401 | C16-H30 | 1.085 | C3-C7-H23 | 118.6 | C16-C14-H28 | 120.3 |
| C7-C10 | 1.384 | C17-H31 | 1.083 | C10-C7-H23 | 120.4 | C12-C15-C13 | 121.2 |
| C7-H23 | 1.083 | C17-C20 | 1.394 | C3-C8-C11 | 121.1 | C12-C15-H29 | 119.5 |
| C8-C11 | 1.392 | C18-H32 | 1.083 | C3-C8-H24 | 120.1 | C13-C15-H29 | 119.3 |
| C8-H24 | 1.083 | C18-H21 | 1.390 | C11-C8-H24 | 118.8 | C12-C16-C14 | 121.2 |
| C9-C13 | 1.397 | C19-H34 | 1.092 | S1-C9-C13 | 120.2 | C12-C16-H30 | 119.5 |
| C9-C14 | 1.398 | C19-H35 | 1.093 | S1-C9-C14 | 120.2 | C14-C16-H30 | 119.3 |
| C19-H33 | 1.095 | C20-C22 | 1.393 | C13-C9-C14 | 119.4 | C6-C17-H31 | 120.0 |
| C20-H36 | 1.084 | C21-C22 | 1.396 | C4-C10-C7 | 120.2 | C20-C17-H31 | 119.7 |
| C21-H37 | 1.084 | C22-H38 | 1.084 | C4-C10-H25 | 119.9 | C6-C18-H32 | 118.7 |
| C21-C18-H32 | 120.9 | C12-C19-H34 | 111.4 | C12-C19-H35 | 111.4 | H34-C19-H35 | 108.2 |
| C17-C20-C22 | 120.1 | C17-C20-H36 | 119.8 | C22-C20-H36 | 120.1 | C18-C21-C22 | 120.0 |
| C18-C21-H37 | 119.9 | C22-C21-H37 | 120.2 | C20-C22-C21 | 119.9 | C21-C22H38 | 120.1 |
| C20-C22-H38 | 120.0 | | | | | | |

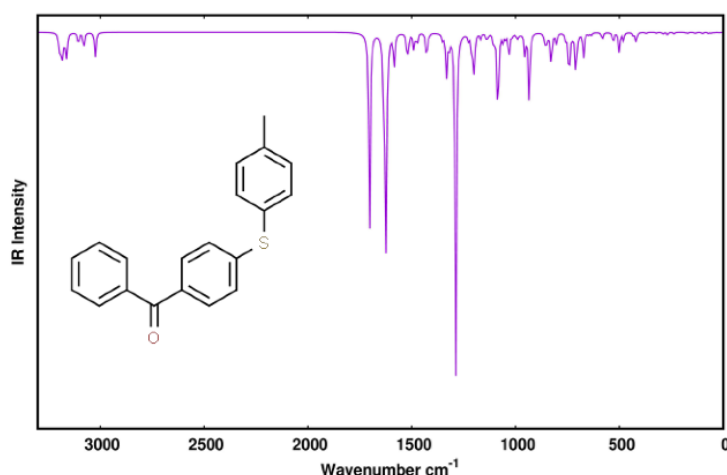


Figure 2. DFT computed IR spectra of 4-4-MPTB molecule

Table 2. DFT computed molecular properties of 4-4-MPTB from B₃LYP/6-311++G(d, p) level of theory.

| Property | Parameter | Property | Parameter |
|-----------------------------|----------------------|----------------------------------|-----------|
| Dipole moment (μ_D) | 5.58 Debye | ΔE_{Gap} | 4.21 eV |
| Polarizability (α) | 40.24 Å ³ | Chemical potential (μ) | -4.0857 |
| Proton affinity (PA) | 939.29 KJ/mol | Chemical hardness (η) | 2.1038 |
| Ionization energy (IE) | 7.75 eV | Softness (σ) | 0.2377 |
| Electron affinity (EA) | 0.54 eV | Electrophilic index (ω) | 3.9762 |
| ϵ_{HOMO} | -6.19 eV | Electronegativity (χ) | 4.0857 |
| ϵ_{LUMO} | -1.98 eV | | |

Vibrational Analysis

IR Spectra

Infrared (IR) spectroscopy measures molecular vibrations, which originates from the stretching and bending of chemical bonds. This technique directly observes functional groups by detecting the stretching and bending of bonds rather than intrinsic properties of the atoms themselves. Each bond type exhibit a distinction vibration frequency, leading to a unique peak in the IR spectrum. IR spectra are straightforward absorption spectra, with the x-axis depicting wavenumber (cm⁻¹) representing the of vibration frequency, and the y-axis indicating absorbance, reflecting the intensity of absorbed IR radiation. Computational calculations based on the B₃LYP/

6-311++G(d, p) Density Functional Theory (DFT) are conducted for frequency analysis and the spectroscopic signature of the 4-4-MPTB molecule. Theoretical calculations reveal that the molecule possesses C1 point group symmetry, with its 38 atoms contributing to 108 modes of fundamental vibrations. The observed IR spectra for 4-4-MPTB and the experimentally obtained spectra are illustrated in Figures 2 and 3, respectively.

Analysis of the theoretical vibrational spectra revealed three prominent peaks within the 2000 and 1000 cm^{-1} range. The peak at 1704 cm^{-1} corresponds to C=O stretching, while peak at 1625 cm^{-1} represents C=C double bond stretching. A sharp peak observed at 1287 cm^{-1} indicates skeletal C-C vibrations. On the left side of the spectrum, smaller absorption peaks with lower intensity are observed around 3000 cm^{-1} , primarily due to C-H stretching. The region below 1200 cm^{-1} , known as 'fingerprint region', is not interpreted in detail as it contains weaker single bonds, mostly involving atoms with higher mass. In this region, where single bond vibrations occur (e.g., C-S stretching), the molecule exhibits a multitude of peaks with low intensity. IR spectroscopy also quantifies the strength of a bond. The investigated molecule displays numerous peaks (low intensity) in the fingerprint region, also providing information about the presence of double bonds and the precise position of C=O absorptions. Experimentally observed IR spectra [15] of 4-4-

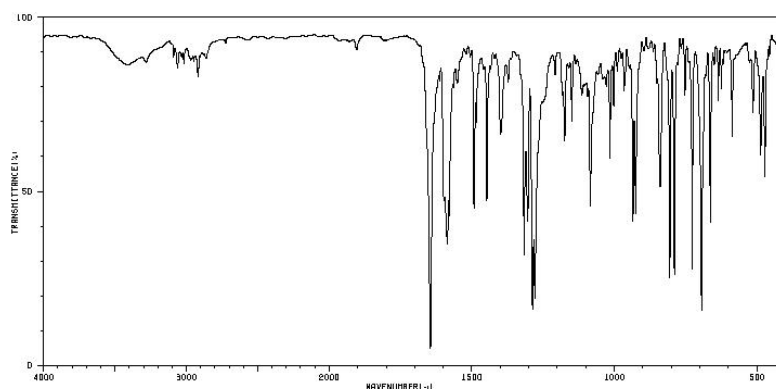


Figure 3. Experimentally reported IR spectra of 4-4-MPTB [15].

MPTB is depicted in Figure 3. The absorption peaks at 1704, 1625, and 1287 cm^{-1} from theoretical calculations align with the experimental peaks at 1650, 1580, and 1280 cm^{-1} . The position of the peaks at 3000 cm^{-1} and in the fingerprint region also corroborate with experimental confirmation. Tokyo Kasei Kogyo Company, Ltd [32], demonstrated C=O, and C=C peaks at 1650 and 1586 cm^{-1} , consistent with the DFT-computed IR spectra.

NBO

Conjugation and delocalization play pivotal roles in influencing the photoinitiating properties of a molecule through various mechanisms. Conjugated systems with extended π -orbitals facilitate efficient overlap with incident light of specific wavelengths, resulting in enhanced light absorption crucial for initiating photochemical reactions. NBO analysis of 4-4-MPTB unveils intramolecular interactions, including hydrogen bonding and hyper-conjugative interactions, which impact

molecular stability and chemical reactivity. These insights provide a deeper understanding of electron density distribution and charge transfer within the molecule. Within the molecular structure of 4-4-MPTB, intriguing patterns of electron delocalization emerge. Natural atomic charges on Sulfur (+0.3023) and C5 (+0.5789) atoms indicate their susceptibility to nucleophilic attack. Similarly, notably negative charges on O2 (-0.5602) and C19 (-0.5910) compared to other atoms make them prone to electrophilic attack. The electron delocalization primarily arises from the conjugation of π -electrons across aromatic rings and the Sulfur atom within the molecule. NBO analysis indicates strong interactions between antibonding orbitals of C4=C11 with corresponding antibonding orbitals of C3=C8 and C7=C10, resulting in the highest energy interactions at 243.22 and 145.30 Kcal/mol, providing significant stabilization. Similarly, C9=C13 exhibits strong interactions with C14=C16 and C12=C15 anti-bonding π -orbitals, with stabilization energy of 233.48 and 198.25 Kcal/mol, respectively. These above donor-acceptor interactions (filled and empty NBO's) are identified based on the highest stabilization energy, as determined by second-order perturbation theory analysis of the Fock matrix.

$$E(2) = \Delta E_{ij} = q_i \frac{F(i, j)^2}{\epsilon_j - \epsilon_i} \quad (5)$$

In the present equation, q_i represents the donor orbital occupancy, ϵ_i and ϵ_j are the diagonal elements (orbital energies), and $F(i, j)^2$ denotes the off-diagonal NBO Fock matrix element. The stabilization energy $E(2)$ is a measure of electron delocalization estimation. Notably, the lone pair on Sulfur, characterized by the lowest occupancy and highest energy, primarily delocalizes into the anti-bonding π -orbitals of adjacent C4-C11, C9-C14, and C9-C13 bonds. Conversely, the lone pair of electrons on Oxygen atom draw very little stabilization energy (18 Kcal/mol) when interacting with nearby antibonding C3-C5 and C5-C6 orbitals. The observed electron delocalization in 4-4-MPTB significantly contributes to its stability and photoinitiating properties.

UV/Vis Spectra

UV/Vis spectroscopy is employed to scrutinize electronic transitions in both organic and inorganic molecules upon absorption of UV or visible light. This method measures the wavelength and intensity of absorbed UV and visible light, providing insights into the electronic structure of the sample molecule. The absorption of radiation results in the promotion of electrons from the ground state to the excited state within the functional group referred to as the 'chromophore'. Each transition occurs between specific energy levels (molecular orbitals), giving rise to peaks in the spectrum. The low energy electronic excited states of 4-4-MPTB molecule are assessed using B₃LYP/6-311++G(d, p) DFT theory. Gas-phase TD-DFT calculations are executed in the singlet state, considering the previously optimized ground-state geometry of the molecule. The calculated UV/Vis spectra of 4-4-MPTB molecule is depicted in Figure 4. The molecule exhibits a robust transition for the excited state 2 at a wavelength 322.78 nm, with an oscillator strength (f) of 0.3616. The highest wave function coefficient for this electronic transition 80→81 corresponds to a nonbonding (n) orbital, typically found on lone pairs, transitioned to π -antibonding ($n \rightarrow \pi^*$) molecular orbital. $n \rightarrow \pi^*$ transitions require less energy to excite the electrons, resulting in absorption peaks appearing at longer wavelength. The second-highest peak coincides with the excited state 8 at a wavelength 258.09 nm, with an oscillator strength of 0.1345. The wave function coefficient for the transition which goes from 75→81 composed of $\pi \rightarrow \pi^*$ orbitals. Electronic transitions such as $\pi \rightarrow \pi^*$ commonly occur in conjugated systems

like double bonds or aromatic rings and typically occur in the UV or blue region. $n \rightarrow \pi^*$ transitions generally manifest in the visible region (purple to red). Higher energy transitions (shorter wavelengths) require more energy and are weaker, resulting in smaller peaks. Higher absorbance or molar extinction coefficient indicates stronger transitions. The investigated molecule can absorb light in the quartz UV region and visible region. Molecules with extended conjugated- π systems display absorption peak shifting to the higher wavelength regions. In conjugated- π systems, the HOMO-LUMO gap decreases, causing absorption to occur in the visible region rather than the UV region. Table 3 showcases the molecular orbitals contributing the electronic transitions, especially $n \rightarrow \pi^*$ and $\pi \rightarrow \pi^*$ excited electronic transitions. The molecules that show delocalization of π -electrons, the absorption in such molecules shifts to longer wavelengths. Therefore, absorption requires less energy as the amount of delocalization

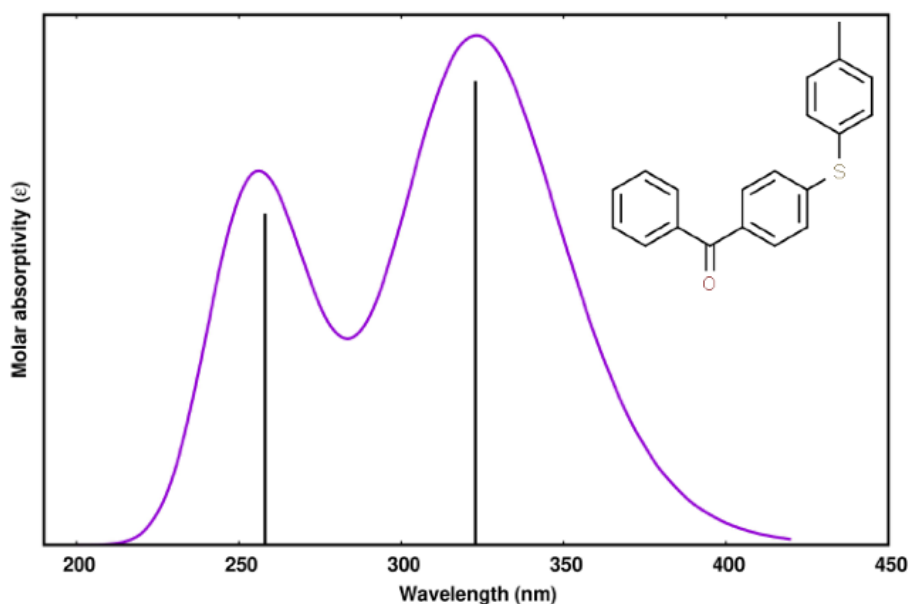
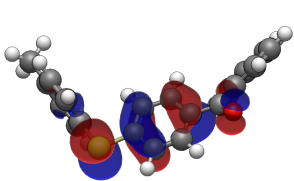
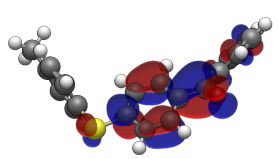
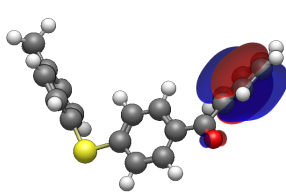
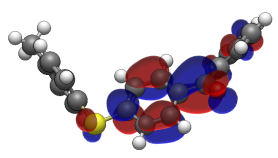


Figure 4. UV/Vis spectra of 4-4-MPTB molecule computed using B₃LYP/6-311++G(d, p) method in gas phase.

increases. There must be less energy gap between bonding and anti bonding orbitals as a result the wavelength absorbed will eventually be high enough to be in the visible region of the spectrum and the molecule will then be seen as coloured. The significant delocalization in 4-4-MPTB places the molecule in the visible region, with a wavelength 322.78 nm.

Table 3. TD-DFT computed excited electronic state properties of 4-4-MPTB in gas phase.

| Excitation energies and oscillator strengths | | |
|--|---|---|
| $\pi \rightarrow \pi^*$ 75→81 f=0.1345 E _{exc} = 4.80 eV λ= 258.09 nm | π -bonding  | π^* -antibonding  |
| $n \rightarrow \pi^*$ 80→81 f=0.3616 E _{exc} = 3.84 eV λ= 322.78 nm | n -non bonding  | π^* -antibonding  |

UV/Vis Spectra in Solvent

When it comes to analyzing molecules using UV-Vis spectroscopy, understanding the solvent's influence is crucial. Water, as a highly polar (dielectric constant~80) and hydrogen-bonding solvent, significantly affects the UV-Vis spectra of molecules compared to studies in gas phase or non-polar environments. Aqueous environments stabilize solute molecules due to solvent-solute interactions, leading to a decrease in energy difference between electronic states. This translates to red shifts (longer wavelengths) in the absorption maxima observed in the UV-Vis spectrum. 4-4-MPTB molecule shows two $\pi \rightarrow \pi^*$ transitions in excited states 2 (74→81) and 7 (78→81), respectively. This leads to lowering the transition energy consequently increasing the wavelengths of transitions which corresponds to visible region, see Figure 5. Similarly, $n \rightarrow \pi^*$ as seen in excited electronic states 1 between 81 and 81 corresponds to considerably higher wavelength 340.29 nm. Water's high dielectric constant significantly impacts electronic transitions in solutes. Polar solvents, for example water, often induce bathochromic shifts. In water, this is seen for n-donors like lone pairs on oxygen, nitrogen, or sulfur atoms. Polar solvents can enhance peak intensity due to increased stabilization of the excited state through solvation, while non-polar solvents generally lead to weaker intensities. A higher intensity peaks are observed in solvent as compared to gas phase for 4-4-MPTB. Table 4 summarises important excited state transitions with energies, oscillator strengths, and wavelengths. Solvent effect is clearly seen in excited electronic state transitions; higher intensity peaks and bathochromic shifts. Figure 5, and table 4 provide a richer understanding of the fascinating world of solvent effects in UV-Vis spectrometry.

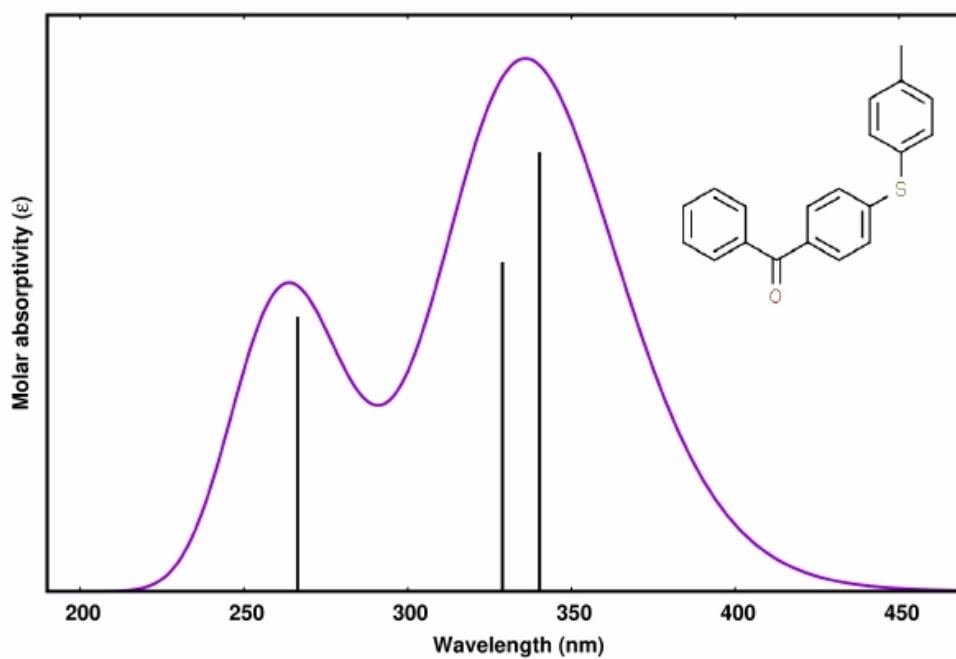
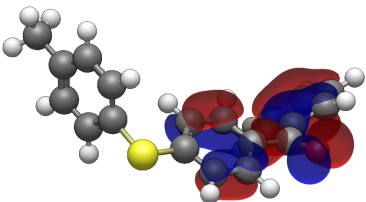
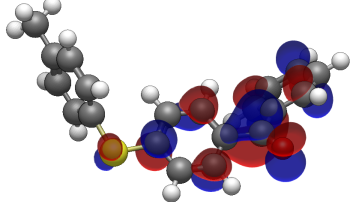
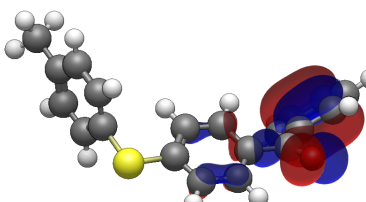
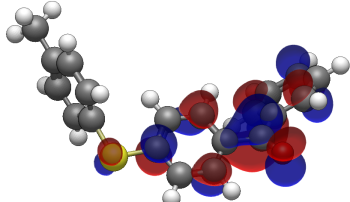
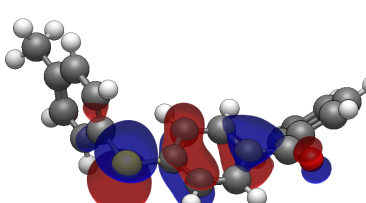
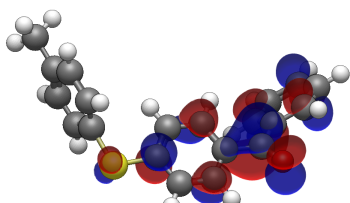


Figure 5. UV/Vis spectra of 4-4-MPTB molecule in aqueous medium computed using B₃LYP/6-311++G(d, p) method.

Table 4. TD-DFT computed excited electronic state properties of 4-4-MPTB in aqueous medium.

| Excitation energies and oscillator strengths | | |
|--|--|---|
| $\pi \rightarrow \pi^*$ 74→81 f=0.1489 E _{exc} = 4.65 eV λ= 266.41 nm | π -bonding  | π^* -antibonding  |
| $\pi \rightarrow \pi^*$ 78→81 f=0.1749 E _{exc} = 3.77 eV λ= 328.96 nm | π -bonding  | π^* -antibonding  |
| $n \rightarrow \pi^*$ 80→81 f=0.3140 E _{exc} = 3.64 eV λ= 340.29 nm | n-non bonding  | π^* -antibonding  |

4. Conclusions

Utilising the B₃LYP/6-311++G(d, p) combination, DFT calculations are conducted to assess the molecular properties of 4-4-MPTB, a benzophenone derivative. Comprehensive analysis of chemical and reactivity attributes influencing the photoinitiating properties of 4-4-MPTB is undertaken and discussed in detail. Chemical reactivity parameters, including chemical potential (μ), Chemical hardness (η), softness (σ), electrophilic index (ω), and electronegativity (χ) are computed from HOMO-LUMO energies in the light of Koopmans approximation. The molecule exhibits high dipole moment and polarizability values, indicating strong intramolecular attractions and enhanced attractive interactions. A low HOMO-LUMO gap signifies high chemical reactivity, facilitating easy transfer from HOMO to LUMO orbitals. Global reactivity parameters suggest that 4-4-MPTB is highly reactive.

IR spectra of the molecule reveal robust peaks at 1625 and 1704 cm⁻¹ for C=C and C=O stretching, aligning with available experimental results. Another sharp peak at 1287 cm⁻¹ corresponds to skeletal C-C vibrations. UV/Vis spectra denote excited state electronic transitions $\pi \rightarrow \pi^*$ and

$n \rightarrow \pi^*$ in quartz UV and visible region of the electromagnetic spectrum with notable peaks at observed at 258.09 and 322.78 nm. Conjugation and delocalization reduce the energy gap between occupied and unoccupied electronic states, causing absorption to shift towards longer wavelengths in the visible region. Understanding the influence of conjugation and delocalization on the photoinitiating properties is pivotal for designing efficient and selective photochemical reactions.

Absorption spectra in solvent, specially an aqueous medium, indicate peaks of excited electronic states with increased intensity and a shift towards longer wavelengths (lower energies) due to strong solvent-solute interactions. Examining solvent effects in detail provides valuable insights into solute behavior, solvent interactions, and the intriguing realm of molecular interactions revealed through UV-Vis spectrometry.

In summary, benzophenone-based photoinitiators remain fundamental to photopolymerization technology, with ongoing efforts addressing current limitations and exploring new frontiers. The quest for environmentally friendly alternatives with extended lifespans and reduced toxicity is ongoing, while exploring the potential of benzophenones in emerging fields like photonics and biomaterials holds exciting promise.

5. Declarations

Ethical Approval

Not applicable

Competing interests

Not applicable

Authors' contributions

Not applicable

Funding

Not applicable

Availability of data and materials

Data is available on request from the author.

References

- [1]. Huang T. L., Li Y. H., Chen Y. C., Benzophenone derivatives as novel organosoluble visible light Type II photoinitiators for UV and LED photoinitiating systems. *J. Polym. Sci.* **2020**; 58: 2914-2925.
- [2]. Qianghua W. & Baojun. Q., Photoinitiating characteristics of benzophenone derivatives as new initiators in the photocrosslinking of polyethylene. *Polym. Eng. Sci.*, **2001**, 41 1220-1226.
- [3]. Altuntaş U., Hitay V., and Özçelik B., Development and Validation of a Rapid Method for Identification and Quantitation of Benzophenone and Related 17 Derivatives in Paper and Cardboard Packaging Materials by Gas Chromatography-Mass Spectrometry. *Packag. Technol. Sci.*, **2016**, 29: 513-524.
- [4]. Suzuki T, Kitamura S, Khota R, Sugihara K, Fujimoto N, Ohta S., Estrogenic and antiandrogenic activities of 17 benzophenone derivatives used as UV stabilizers and sunscreens. *Toxicol. Appl. Pharmacol.* **2005**;203:9e17.
- [5]. Feng C., Wang Q. L., Liu F., Zhang B., Synthesis and Application of New Benzophenone Photoinitiators, *Chem. Select*, **2023**, 8, e202302572.
- [6]. Liska R., Industrial Photoinitiators: A Technical Guide. by W. Arthur Green. *Chem. Phys. Chem.*, **2011** 12: 1389-1389.
- [7]. Huang T. L., Chen Y. C., Synthesis and free radical photopolymerization of one-component type II photoinitiator based on benzophenone segment, *J. Photochem. Photobio. A*, **2022**, 429 113900.
- [8]. Jimenez-Díaz I, Zafra-Gomez A, Ballesteros O, Navalón A., Analytical methods for the determination of personal care products in human samples: an overview. *Talanta* **2014**;129: 448e58.
- [9]. Żaneta B., Igor T., Paweł G., Beata B., Alicja S., Alicja M., Grzegorz K., Bogusława B., Benzophenone-2 exerts reproductive toxicity in male rats, *Reprod. Toxicol.* 120, **2023**, 108450.
- [10]. Gokhan T., Burak E., Meral A., Demet K. B., Nergis A, Photopolymerization and photophysical properties of amine linked benzophenone photoinitiator for free radical polymerization, *J. Photochem. Photobio. A*, **2011**, 219 26-31.
- [11]. Huang T. L., Li Y. H., Chen Y. C., Benzophenone derivatives as novel organosoluble visible light Type II photoinitiators for UV and LED photoinitiating systems. *J. Polym. Sci.* **2020**; 58: 2914-2925.
- [12]. Ying W., Pu X., Gang Q. W., Su Q. S., Jun N., Photopolymerization induced by a benzophenone derivative photoinitiator, *Chin. Chem. Lett.*, **2007**, 18 977-980.

- [13]. Huang T. L., Chen Y. C., Synthesis and free radical photopolymerization of one-component type II photoinitiator based on benzophenone segment, *J. Photochem. Photobio. A*, **2022**, 429 113900.
- [14]. Ramirez K., Orrantia-Borunda, E., Flores N., Calculation of global and local reactivity descriptors of Carbodiimides, a DFT study. *J. Theor. Comput. Chem.* **16** **2017**.
- [15]. Chemical Book, 4-(4-Methylphenylthio)benzophenone, https://www.chemicalbook.com/SpectrumEN_83846-85-9_IR1.htm, (Accessed 20 December 2023)
- [16]. Aravindhyan R., Jianping Hu, Momeen M. U., Role of the solvent polarity on the optical and electronic characteristics of 1-iodoadamantane. *RSC Adv.* **2023** 9;13(42):29489-29495.
- [17]. Giovannini, T., Egidi, F., & Cappelli, C. (2020). Molecular spectroscopy of aqueous solutions: a theoretical perspective. *Chem. Soc. Rev.*, **2020**,49, 5664-5677.
- [18]. Bendjeddou, A., Abbaz, T., Gouasmia, A., Villemin, D., Quantum Chemical Studies On Molecular Structure and Reactivity Descriptors of Some P-Nitrophenyl Tetrathiafulvalenes by Density Functional Theory (DFT). *Acta Chim. Pharm. Indica.* **6**. **2016** 32-44.
- [19]. Mendoza-Huizar, L., Global and local reactivity descriptors for picloram herbicide: A theoretical quantum study. *Química Nova.* **38**. **2015** 71-76.
- [20]. Biswarup M., Umasankar S., Bhudeb R. D., The Ground State Comparative Study of Proton Affinities and Associated Parameters of Conjugated α , β -unsaturated Carbonyl Compounds in Gas and Aqueous Phases by Density Functional Theory Method, *Indian J. Adv. Chem. Sci.*, **4**(4) **2016** 401-408.
- [21]. Lee C., Yang W., and Parr R. G., Development of the Colle-Salvetti correlation-energy formula into a functional of the electron density. *Phys. Rev. B*, **1988** 37, 211-212.
- [22]. Frisch, M. J., Trucks, G. W., Schlegel, H. B., Scuseria, G. E., Robb, M. A., Cheeseman, J. R., Scalmani, G., Barone, V., Petersson, G. A., Nakatsuji, H., Li, X., Caricato, M., Marenich, A. V., Bloino, J., Janesko, B. G., Gomperts, R., Mennucci, B., Hratchian, H. P., Ortiz, J. V., Izmaylov, A. F., Sonnenberg, J. L., Williams-Young, D., Ding, F., Lipparini, F., Egidi, F., Goings, J., Peng, B., Petrone, A., Henderson, T., Ranasinghe, D., Zakrzewski, V. G., Gao, J., Rega, N., Zheng, G., Liang, W., Hada, M., Ehara, M., Toyota, K., Fukuda, R., Hasegawa, J., Ishida, M., Nakajima, T., Honda, Y., Kitao, O., Nakai, H., Vreven, T., Throssell, K., Montgomery, J. A., Jr., Peralta, J. E., Ogliaro, F., Bearpark, M. J., Heyd, J. J., Brothers, E. N., Kudin, K. N., Staroverov, V. N., Keith, T. A., Kobayashi, R., Normand, J., Raghavachari, K., Rendell, A. P., Burant, J. C., Iyengar, S. S., Tomasi, J., Cossi, M., Millam, J. M., Klene, M., Adamo, C., Cammi, R., Ochterski, J. W., Martin, R. L., Morokuma, K., Farkas, O., Foresman, J. B., and Fox, D. J. Gaussian 16 Revision C.01, Gaussian Inc. Wallingford CT, **2016**.
- [23]. Duca G., Bolocan N., Understanding the Chemical Reactivity of Dihydroxyfumaric Acid and its Derivatives through Conceptual DFT, *Rev. Chim.*, **72**(4), **2021**, 162-174.

- [24]. Singh J., IR and Raman spectra with Gaussian-09 molecular analysis of some other parameters and vibrational spectra of 5-fluoro-uracil. *Res. Chem. Intermed.*, 46. **2020** 2457–2479.
- [25]. Ellis, A. M., and Mayhew, C. A. In *Proton Transfer Reaction Mass Spectrometry Principles and Applications*; *John Wiley & Sons*, Chichester, United Kingdom: **2014**.
- [26]. Koopmans, T., Ordering of wave functions and eigenvalues to the individual electrons of an atom. *Physica*, **1934**, 1, 104-110.
- [27]. Selvaraj, S., Rajkumar, P., Kesavan, M., Gunasekaran, S., Kumaresan, S., Experimental and theoretical investigations on spectroscopic properties of tropicamide. *J. Mol. Struct.* 1173 **2018** 52-62.
- [28]. Dixit V., Yadav R. A., DFT-B₃LYP computations of electro and thermo molecular characteristics and mode of action of fungicides (chlorophenols), *Int. J. Pharm.* 491 **2015** 277-284.
- [29]. Chattaraj P. K., Sarkar U., Roy D. R., Electrophilicity Index. *Chem. Rev.*, **2006** 106, 2065-2091.
- [30]. Balachandran V., Rajeswari, S., Lalitha S., Vibrational spectral analysis, computation of thermodynamic functions for various temperatures and NBO analysis of 2,3,4,5-tetrachlorophenol using ab initio HF and DFT calculations. *Spectrochimica acta. Part A, Molecular and biomolecular spectroscopy*, 101, **2013** 356–369.
- [31]. Muthu, S., Renuga, S., Molecular orbital studies (hardness, chemical potential, electronegativity and electrophilicity), vibrational spectroscopic investigation and normal coordinate analysis of 5-{1-hydroxy-2-[(propan-2-yl)amino]ethyl}benzene-1,3-diol. *Spectrochimica acta. Part A, Molecular and biomolecular spectroscopy*, 118 **2014** 683–694.
- [32]. SpectraBase, Tokyo Kasei Kogyo Company, Ltd., Tokyo, Japan, <https://spectrabase.com/spectrum/ELVtqpzdIL>, (Accessed 20 December 2023).